

MODELING ALFA PULSAR SURVEYS: THE CORNELL APPROACH

W. H. T. VLEMMINGS¹ AND J. M. CORDES¹

Version v7.0; 04-07-05

ABSTRACT

We consider metrics for survey success and apply them to potential ALFA pulsar survey strategies. ALFA precursor surveys are modeled for various pointing schemes and observational setups. We describe the modeling procedure and discuss the results for both normal pulsars as well as millisecond pulsars. We find that:

- A sparse sampling approach with the same number of pointings as a dense pointing scheme dramatically increases (by 50%) the number of detected pulsars, at the expense of missing some of the weaker pulsars.
- Due to the high sidelobes of the ALFA beam, for the same number of pointings, a sparse sampling approach surveys 1.73 times the volume of the dense sampling approach.
- Due to the combined effects of nulling and scintillations, we find that a dual-pass approach that uses half the observing time in each pass of a single-pass approach increases the number of detections by ≈ 6 -10%, which increases to 11-12% when the second pointing is offset by one-half beamwidth (FWHM/2).
- The percentage of detections for millisecond pulsars is increased by an additional $\approx 5\%$ in the dual-pass approach.
- When a single, rare and weak object in the pulsar population is sought, we find that a dual-pass approach is superior to a single-pass approach. Using a dual-pass approach, the chance of detecting a single, rare object which is nulling 50% of the time increases by 5-10%.

Our recommendations are that:

- The survey use an initial sparsely sampled grid that is filled in later.
- The survey should use the dual-pass approach. This will not only increase the number of detections by a small amount, but will also increase the detection chance of rare objects. Additionally, the dual-pass approach can serve as an immediate confirmation of most of the less variable pulsars.

Subject headings: ALFA pulsar survey modeling

1. SIMULATIONS AND SURVEY METRICS

This document discusses simulations that were designed to test alternative survey designs that use the ALFA system. Most pulsar simulations are characterized assuming that the pulsed flux density is constant and that radiometer noise is the only obstacle to detection. In reality, pulsars rarely show constant pulsed flux density. Instead, the signals we measure vary due to a variety of effects, including intrinsic modulations, orbital eclipses, and extrinsic propagation effects. Our simulations include all of these effects to varying degrees of sophistication. Our simulations also differ in the way that pseudo pulsar populations are generated. In particular, our approach models the pulsar beam and its true luminosity and then produces simulated average pulses according to random distributions of angles between spin and magnetic axes and the line of sight (LOS).

As a survey metric or figure of merit, the total number of pulsars detected is implicitly invoked in most studies. The intuitive justification is that discovery of the most interesting objects (relativistic binaries, millisecond pulsars, etc.) scales with the total number. We consider several survey metrics that are most likely optimized through different observing strategies and processing and involve maximization of the number of:

1. pulsars of any kind (young, high-field, MSPs, etc.);

2. young, high-field objects;
3. MSPs of any period;
4. relativistic binaries (PSR-NS, PSR-PSR, and PSR-BH);
5. MSPs with $P < 1.5$ ms and especially sub-ms MSPs;
6. pulsars with magnetar-like magnetic fields;
7. very rare objects that are extreme members of the above categories or of ones not yet thought of; for some of these there may be only one or two in the Galaxy.

While we do not explicitly model all of these categories, we do quantify surveys according to how many pulsars they detect and also whether a survey strategy can detect a one-of-the-kind type object.

To maximize sheer numbers of sources of any type in a survey, it is well known that telescope time is better used to cover more solid angle rather than by integrating longer to reach greater distances: the volume searched is thus maximized. Built-in assumptions to this approach are (1) that the survey is noise limited and (2) the targeted source population spans solid angles that can be surveyed to a greater extent. It also assumes in effect the large-source-number limit: there are large numbers of objects to be detected and so any volume in the source domain is as good as any other. If there is insufficient telescope time to cover all solid angles with dense sampling, one can do better with a sparse sampling approach, as shown below.

However, in the small-source-number limit where, say, there is only one PSR-BH binary in the Galaxy at unknown

¹ Department of Astronomy, Cornell University, Ithaca, NY 14853; wouter@astro.cornell.edu.

location, a different approach must be taken. One must cover ALL volume in the search domain with sufficient sensitivity to find the object. In this case, a survey can profitably make use of dense sampling schemes and repeated observations. We analyze this situation below through simulations of a singular “hot object.”

2. MODELS AND SIMULATIONS

Modeling was performed using our pulsar simulation and detection code with the ALFA parameters of the precursor survey (256 channels, 100 MHz bandwidth). For the pulsar evolution we used a model based on ACC but including torque decay of 6 Myr. This model reproduces, as a first approximation, the P-Pdot diagram best. The modeling procedure is described in more detail in the Appendix. Additionally, the Appendix also includes a discussion on the ALFA beam shape.

We considered the following pointing procedures:

- 1.) Filled sampling (as in Fig. 1); the beams overlap at approximately the half-power point.
- 2.) Sparse sampling (only pointing nr.2 in Fig. 1); this exploits the side-lobes, as beams and subsequent pointings are separated by $\sqrt{3} \times \text{FWHM}$; total number of pointing remains the same.
- 3a.) 2 passes with half the integration time with identical sampling.
- 3b.) 2 passes with half the integration time shifted by $\text{FWHM}/2$; For the sparse sampling we chose a shift of half the pointing separation.

For the single passes the integration time $t = 300$ s, for the dual passes $t = 150$ s. Variability was included as diffractive and refractive interstellar scintillation (DISS, RISS), and nulling, which can also be taken as a proxy for eclipses in some binary pulsars. RISS appears as long-term modulations (days to years) of the pulsar flux that have roughly a symmetric distribution. DISS modulations are faster (seconds to hours) and have a broad, exponential distribution that tends toward a narrow, narrow distribution as the number of scintles in the frequency-time plane of an observation increases. For nulling, we assume that 20% of the pulsars null and assume that there is a 20% chance that the nulling pulsars are off for the entire duration of the observation. In our simulations, we generate modulations for both DISS and RISS, g_{iss} and g_{iss} , respectively. The distribution of the variability factor $g = g_{\text{iss}}g_{\text{iss}}$ is shown in Fig. A4. An additional test was performed with the cycle time (time between the overlapping pointings) less than a characteristic scintillation time scale of 300 s.

Table ?? summarizes the results, with the detection fraction normalized to the number of pulsars detected with a threshold of 10 in the single 300 s pass. For the dual-pass models we considered sources that were detected at a threshold of 7.5 combining both passes and sources that were only detected in one of the two passes at a threshold of 10.

To assess the percentage of ‘new’ detections we also examined the percentage of objects detected below the half-power level of the Parkes Multi-Beam survey for the different pointing schemes (even though the PMB survey did not cover the entire Arecibo sky). The results of these tests are also shown in Table. ?? as well as in Fig. 2

2.1. Hot-Object test

TABLE 1
MODEL RESULTS

Model	total pulsars (normalized)	dual-pass detec. (threshold = 7.5)	1 pass detec. (threshold = 10)	New Objects % of total	Hot Objects % of total
1	1.00	-	-	67%	17%
2	1.49 ± 0.05	-	-	57%	6%
3a (dense)	1.06 ± 0.04	0.58	0.24	66%	22%
3b (dense)	1.11 ± 0.04	0.51	0.30	66%	23%
3a (sparse)	1.66 ± 0.05	0.87	0.39	56%	7%
3b (sparse)	1.92 ± 0.08	0.38	0.77	56%	8%

TABLE 2
MSP MODEL RESULTS

Model	total pulsars (normalized)	dual-pass detec. (threshold = 7.5)	1 pass detec. (threshold = 10)	New Objects % of total
1	1.00	-	-	77%
2	1.53 ± 0.05	-	-	70%
3a (dense)	1.12 ± 0.03	0.39	0.36	75%
3b (dense)	1.16 ± 0.03	0.37	0.40	76%
3a (sparse)	1.69 ± 0.05	0.69	0.50	68%
3b (sparse)	1.89 ± 0.07	0.29	0.80	62%

We did a separate test to investigate the efficiency of the pointing schemes outlined above to detect ‘hot-object’ which have been classified as being a source which is detected at a $S/N = 12$ when the main ALFA beam is pointed directly at it at small zenith angle for a 300 s observation. The resulting detection probability is shown in Table.1, when the standard RISS, DISS variability and nulling is taken into account. Obviously, when the source is not affected by variability, the dual-pass (150 s) scans will only detect the sources at the same threshold when we use the identical pointing scheme. We repeated the same tests for a hot-object at $S/N = 12$ for a 150 s pointing. The hot-object test was performed for both an object the has a nulling efficiency of 20% as well as for one with an efficiency of 50%. The results for the 50% nulling hot-object are included in Table.1.

2.2. Millisecond Pulsars

Millisecond pulsars (MSPs) were modeled using the pseudo-luminosity law, period distribution, velocity distribution and disk scale height from Cordes & Chernoff (1997). We modeled the full Arecibo sky with $|b| < 50$ degrees. The detection cumulative distribution function is shown in Fig. 3. The modeling results are given in Table. ??.

3. SUMMARY OF SIMULATION RESULTS

- The sparse sampling scheme will, in the same amount of pointings, increase the number of detected pulsars by $\approx 50\%$. While the number of pulsars detected per square degree decreases by a factor of 2, the area sampled increases by a factor of 3. The median flux of the detected pulsars however, will be higher in the sparse sampling, as mostly the stronger pulsars will be detected in the beam side-lobes. This reduces the percentage of detected ‘new’ pulsars, but due to the 55% increase in total number, the effective number of detected ‘new’ pulsars still increases.

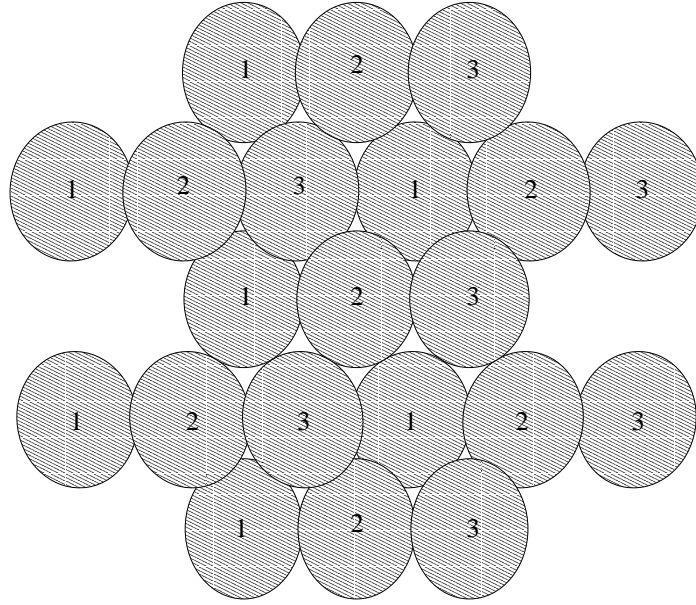


FIG. 1.— One of the blocks of the ALFA pointing pattern.

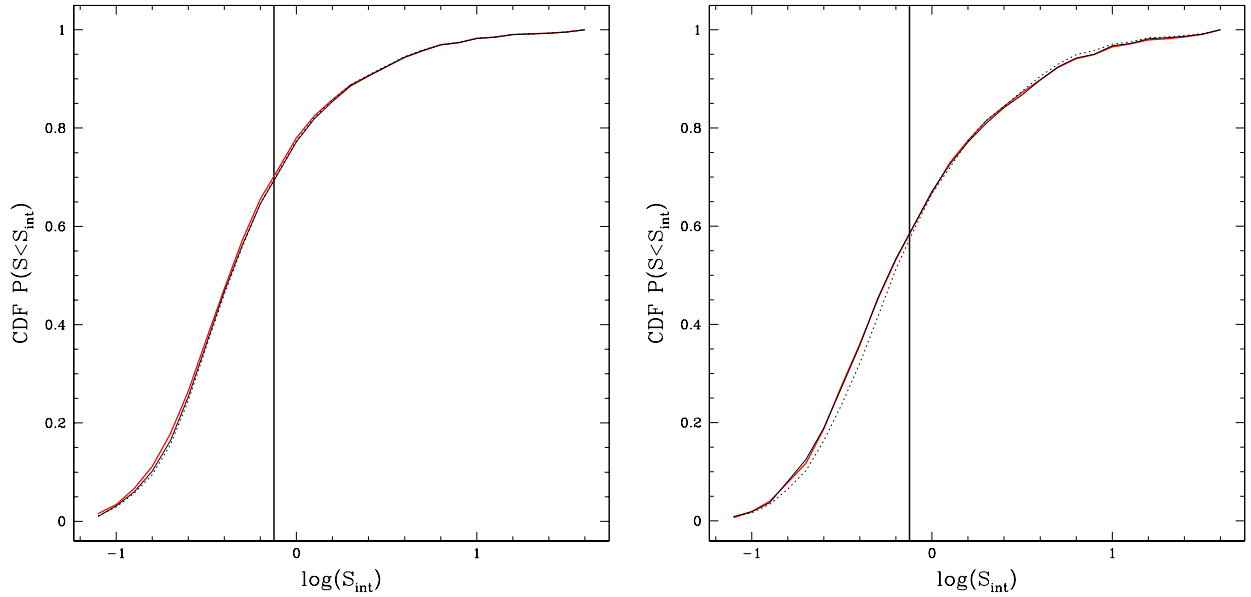


FIG. 2.— (left) The (normalized) cumulative distribution function for the dense sampling scheme. The thick (red) line is a single 300s pass. The thin line is pointing scheme 3a and the dotted line is scheme 3b. The vertical line denotes the flux cutoff below which the pulsars are classified as ‘new’ detections (right) Similar for the sparse sampling scheme.

- An additional sparse sampling of the survey area, which can be filled in by later pointings, will detect $\approx 50\%$ of the pulsars.
- If $\approx 20\%$ of the pulsars null with a nulling efficiency of 20%, the multiple pass approach (at identical positions) will improve the number of detection by approximately 5-10% if detections at a threshold equal to the long scan threshold (10) in one of the two scans are included. If no nulling is included in the models, multiple passes still improve the number of detections by $\approx 5\%$. Additionally, multiple passes will detect some of the objects that are most affected by scintillation at the cost

of losing some of the fainter pulsars. The increase is similar in the case of sparse sampling using the high ALFA sidelobes. The percentage of ‘newly’ detected pulsars is decreased by approximately 5 percent. As a result, the absolute number of ‘new’ objects detected in the dual-pass approach is similar to those detected in the one pass approach.

- Performing a second pass off-set by $0.5 \times \text{HPBW}$ from the first pass seems to increase the number of detection only slightly in both the densely and sparsely sampled case (the offset is larger in the sparse sampling case). Where the identical sampling picks up most of the pul-

sars in both passes, the off-set sampling has more detections in one of the two passes.

- There is no significant difference in the number of detection when taking into account cycle times faster than a typical scintillation time (in this case 300 s).
- In the hot-object test, with the hot-object defined to have $S/N=12$ for the 300 s pass, the object is detected approximately 15% of the time, with no noticeable difference between the pointing schemes, when variability is included. This assumes a nulling efficiency of 20% and that the object is placed randomly in the area surveyed with the sparse sampling and assuming a randomly selected distance out to approximately 10 kpc. If the object is not subject to significant variability, the off-set multiple pointings will fail to detect it (at a threshold of 10), as the 150 s integration time for each off-set pass is not sufficiently long. When the nulling efficiency is increased to 50%, the detection probability increases by 5-10% in the dual-pass approach.
- When the hot-object is defined to be at a $S/N=12$ for the 150 s pass with a nulling efficiency of 50%, the detection probability of nearby objects (subject to ISS variability) $\approx 15\%$ in the single pass approach. While for those object at larger distances that are less affected by variability the detection percentage is $\approx 20\%$. For the multi-pass approach, in both cases the detection probability increases by $\approx 5 - 10\%$
- Comparable but somewhat higher than for the normal pulsars, approximately 15% more millisecond pulsars are detected in the multi-pass scheme, even though the median flux is higher in that case. This is due to the fact that the detectable MSPs are somewhat closer than the regular pulsars and are thus more affected by scintillation. As a result, the median distance of the newly detected MSPs is approximately 5-10% less in the dual-pass approach. Approximately 80% of the millisecond pulsars are labeled as 'new' pulsars in a single 300 s pass, while approximately 75% of the pulsars in the dual-pass schemes are labelled as new. Because more millisecond pulsars are detected with two passes, the absolute number of 'new' detections higher in the dual-pass scheme.

4. RECOMMENDED BEST APPROACH

The dual-pass approach with an initial sparse grid is preferable as:

- The number of detections improves by $\approx 10\%$, with the off-set second pointings providing the most improvement. This is only slightly dependent on the assumption that approximately 20% of the pulsars null. In the

limiting case of no nulling, the detection percentage increases by a few percent less ($\approx 3-5\%$ increase).

- While the median flux in the dual-pass approach is higher and the resulting detection percentage of 'new' objects is slightly lower, the total number of 'new' detections is somewhat larger, due to the increased number of detections.

TABLE 3
SURVEY PARAMETERS

Obs. frequency ν	1.4 GHz
Bandwidth	100 MHz
nr. of channels	256
dwelt time	300 s (one-pass) / 150 s (dual-pass)
S_{sys} (center beam)	3.7 Jy
S_{sys} (outer beams average)	4.7 Jy
Approx. sky coverage in dense sampling in 100 hrs with 70% efficiency	18 deg ² with Gain > 4.5 K/Jy
Same with sparse sampling (using side-lobes)	54 deg ² with Gain > 1-2 K/Jy
Search Volume Ratio	
Sparse/Dense sampling (same number of pointings)	1.73

- Mostly the same considerations apply for millisecond pulsars, however, the dual-pass approach has a higher gain for MSPs (15%)
- Assuming a heavily nulling hot-object, the dual-pass approach significantly improves the chance to detect this rare object
- The sparse sampling approach increases the number of detected pulsars significantly (50%) when using a similar number of pointings.
- An initial sparse grid which can be filled later will already detect 50% of the pulsars.
- In the 'hot-object' test, the sparse approach fares equally well as the dense sampling approach only IF we assume that the sparse approach covers more area in the same number of pointings, and if the single hot-object is located in the area of the sky covered in the sparse sampling. This is because the dense approach covers a factor of 3 less area.
- If however, the sparse approach is simply the initial pass, it is 3 times less likely to detect the hot-object.
- Finally, the dual-pass approach can serve as an immediate confirmation for some of the stronger, less variable pulsars.

APPENDIX

THE CORNELL MODELING PROCEDURE

Orbit Code

In the first step, a catalog of n pulsars is created using the orbit-code by Dave Chernoff, which was used by Cordes & Chernoff (1998) and Arzoumanian, Chernoff & Cordes (2002; ACC). The Galactic potential has a 3-component disk distribution to simulate the molecular ring and/or central bulge. The components are flat in density between: 1) 0-1500 pc, 2) 1500-3000 pc and 3) 3000-13000 pc. The relative weights for the density distributions can be set (now set to 2 : 4 : 1. Spiral arms are hardcoded

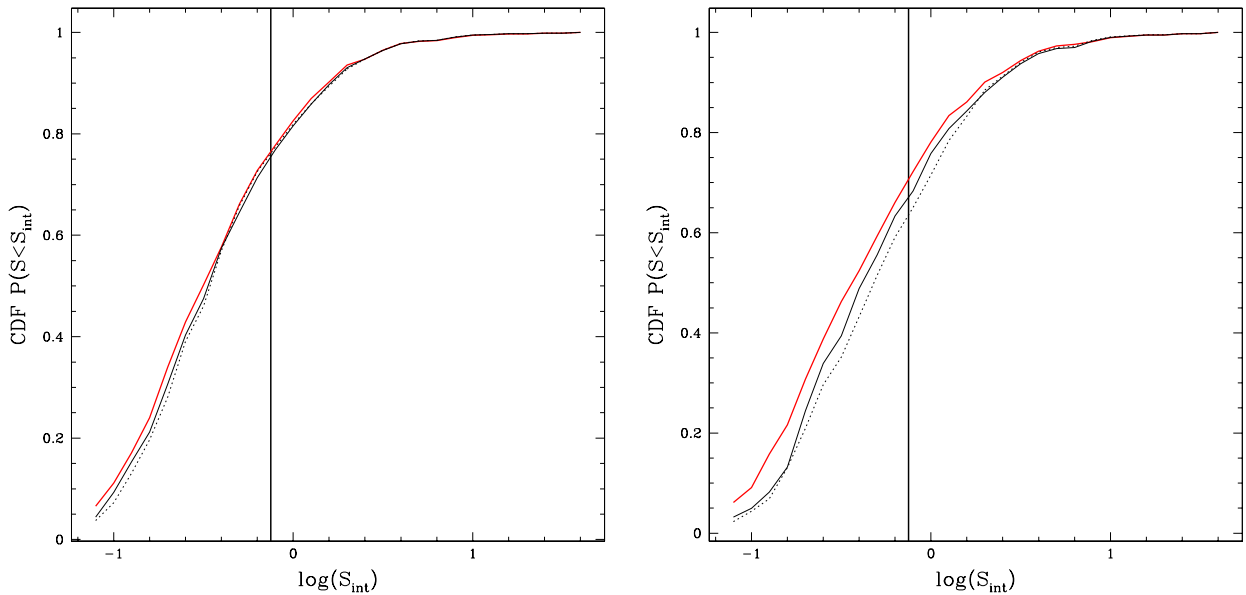


FIG. 3.— The (normalized) cumulative distribution function for the dense (left) and sparse (right) sampling scheme observing a modeled sample of MSPs. The thick (red) line is a single 300s pass. The thin line is pointing scheme 3a and the dotted line is scheme 3b. The vertical line denotes the flux cutoff below which the pulsars are classified as ‘new’ detections.

in the outer region and can be set to have an increased SN rate. The average SN rate per are (1,2 and 3) are fixed. The maximum age has been set to 50 Myr. The output from this Monte-Carlo code contains the pulsar positions, velocities and age.

Properties of Pseudo Pulsars

The next step consists of determining the observational properties of the pulsars created with the orbit code. At the same time a first selection is made for the pulsars that will be observable with the telescope and survey of choice after supplying the code with information on the telescope latitude, system temperature, gain, observing frequency, bandwidth, number of channels and polarizations, correlation time, scan time and the threshold number. As the ALFA system gain is not uniform for all the beams, and temporal intensity fluctuations will be included in the models as well, this first cut will be based on a significantly higher gain and lower threshold than the real survey.

The initial period P_0 and initial torque constant k_0 are selected from birth distributions and then evolved according to a predetermined spindown model. This leads to the current P and \dot{P} and beam luminosity using the age from the orbit calculations. We use a slightly modified version of the Arzoumanian, Chernoff & Cordes (ACC, 2002) model, which includes a 6 Myr torque decay time. This model was found to reproduce the P, \dot{P} -diagram best (although still not perfectly). The pulsar beaming parameters are calculated using the beaming model from ACC. Position and distance are taken from the orbit calculations which are used to get DM and scattering measure (SM) from the NE2001 model. From these we calculate the pulse-broadening time, which has a major influence on pulse width and, hence, on the number of harmonics detected. We also calculate the scintillation bandwidth and time $\Delta\nu_d$ and Δt_d used to calculate the DISS scintillation modulation, g_{iss} . Using these and the survey parameters, the harmonic sum is calculated which is then compared with the surveys threshold times the rms-noise.

The output file contains the galactic coordinates l, b , the distance, dispersion measure, age, P, \dot{P} , the pulsar beam flux densities, harmonic sum, zenith angle, velocities, and scintillation parameters.

Applying ALFA Survey Selections

Using the observables determined in the previous steps, the ALFA observations are modeled using a detailed model for the beam shape and gaincurves of the multi-beam system. This is described in somewhat more detail below. The survey parameters are given in Table. ???. The ALFA code can be run for any range in galactic coordinates using any pointing pattern. For these models we assume the pointing is observed at transit. We include the gain dependence on the pointing elevation. Additionally, it can simulate feed tracking (rotation) during each scan (for scans less than or equal to 300 sec this is found to have negligible effect). Furthermore, the simulations include scintillation and nulling effects or various combinations of these. Nulling is described by a 20% fraction of nulling pulsars which have probability of being *off* for 20% of the time. RISS is quantified by a log-normal distribution with $\sigma_{\text{riiss}} = 0.1$. The DISS is quantified by a Gamma distribution with N degrees of freedom. Where N is given by

$$N \approx (1 + 0.1T/\Delta t_d) * (1 + 0.1B/\Delta \nu_d) \quad (\text{A1})$$

Here, T is the total on source observing time and B is the total bandwidth. The variability effects are then combined in the variability factor g . The distribution of g for RISS and DISS is shown in Fig. A4.

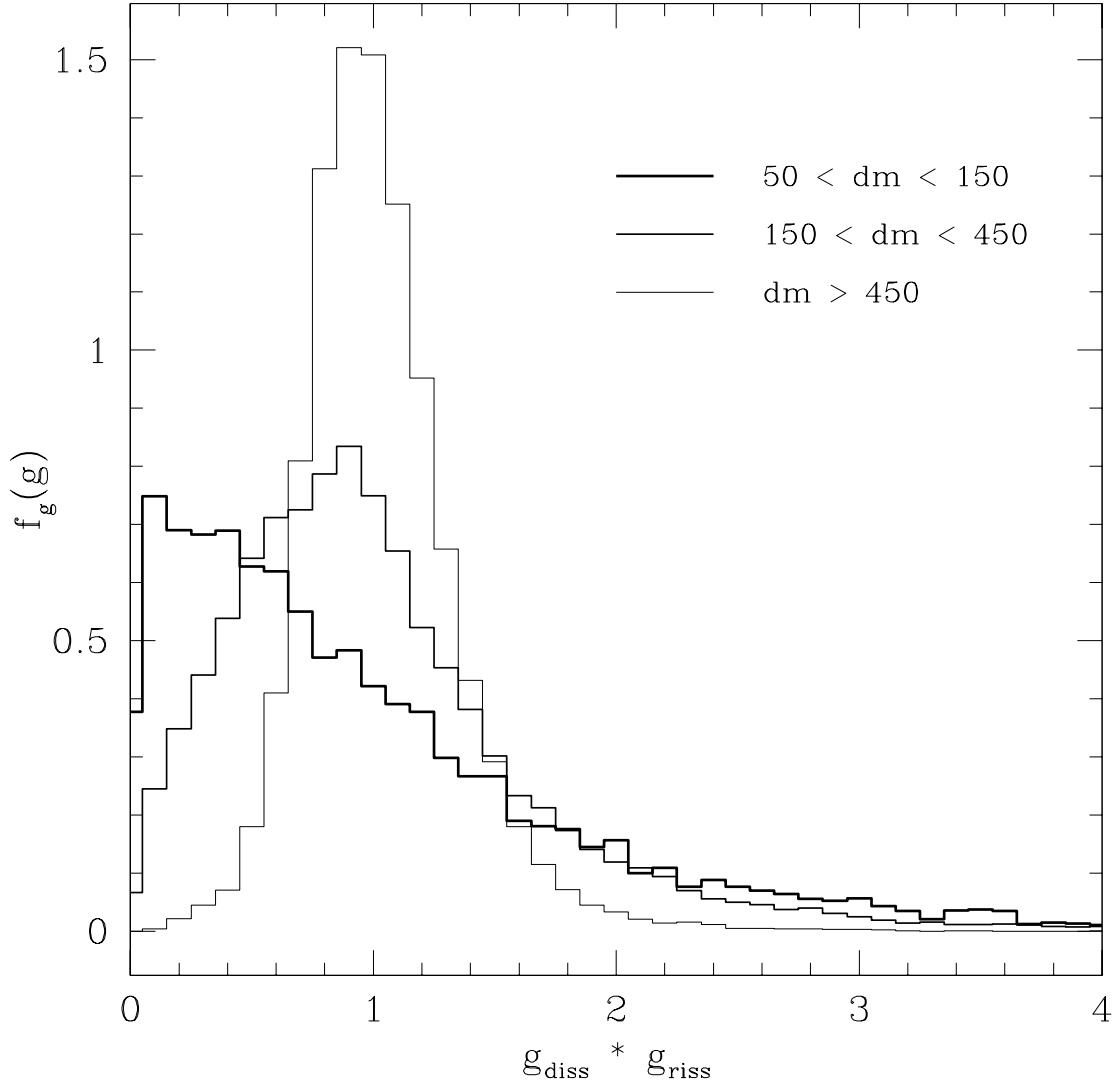


FIG. A4.— The distribution of variability factor $g = g_{\text{DISS}} \times g_{\text{RISS}}$ at 1.4 GHz for 3 different ranges of DM of the modelled pulsars (before applying survey selection). The distribution has unit area. For the lowest DM range, DISS is unquenched by time-bandwidth averaging, and dominates g , which thus shows an exponential distribution with 100% modulation. Larger DM s correspond to progressively greater time-bandwidth quenching of DISS, leading to a narrower and more symmetric distribution centered on $g = 1$.

THE ALFA BEAMS

The footprint of the ALFA beam used in the modeling is shown in Fig. B5 for the combination of the 7 beams and for one of the separate beams. The beams are described by elliptical Airy functions with a first order coma correction with the parameters taken from the “*Final Feed Selection Study*” (ALFA memo 02-08) using spline fits to the tabulated values. To create the composite image of all the beams, we use for each sky position the most sensitive beam at that point.

Of the 7 beams, the outer beams have a large coma contribution that significantly increases the sidelobe level. The first sidelobe is at approximate -8.7 dB which corresponds to approximately 70% of the GBT sensitivity. To illustrate the effect of the coma, we have determined the pulsar detection PDF and CDF as a function of distance r_{uv} between the center of the detecting beam and the pulsar position. In Fig. B6, we show the PDF and CDF for the 7 beam system using the best beam model as well as using a standard Airy function and a beam model with a 5 times as strong coma effect. In this figure we include pulsar detections in multiple beams, thus many pulsars are counted multiple times as they are detected in both the sidelobe of one beam as well as in the main part of another. For the correct beam description, 16.5% of the pulsars are detected in the sidelobes, while for a standard Airy beam this is only 6.5%. For beams with the increased coma effect this increases to 39.5%.

In Fig. B7 we show a plot similar to Fig. B6 counting only the best detections (detections at highest sensitivity) for the dense and the sparse sampling approach. In the dense approach the beams overlap at approximately the half-power point and thus most pulsars are detected within the half-power level. The very few pulsars detected in the sidelobes (less than 0.5%) are due to pointings at the edge of our survey region. In the sparse approach the beams do not overlap significantly, and the number

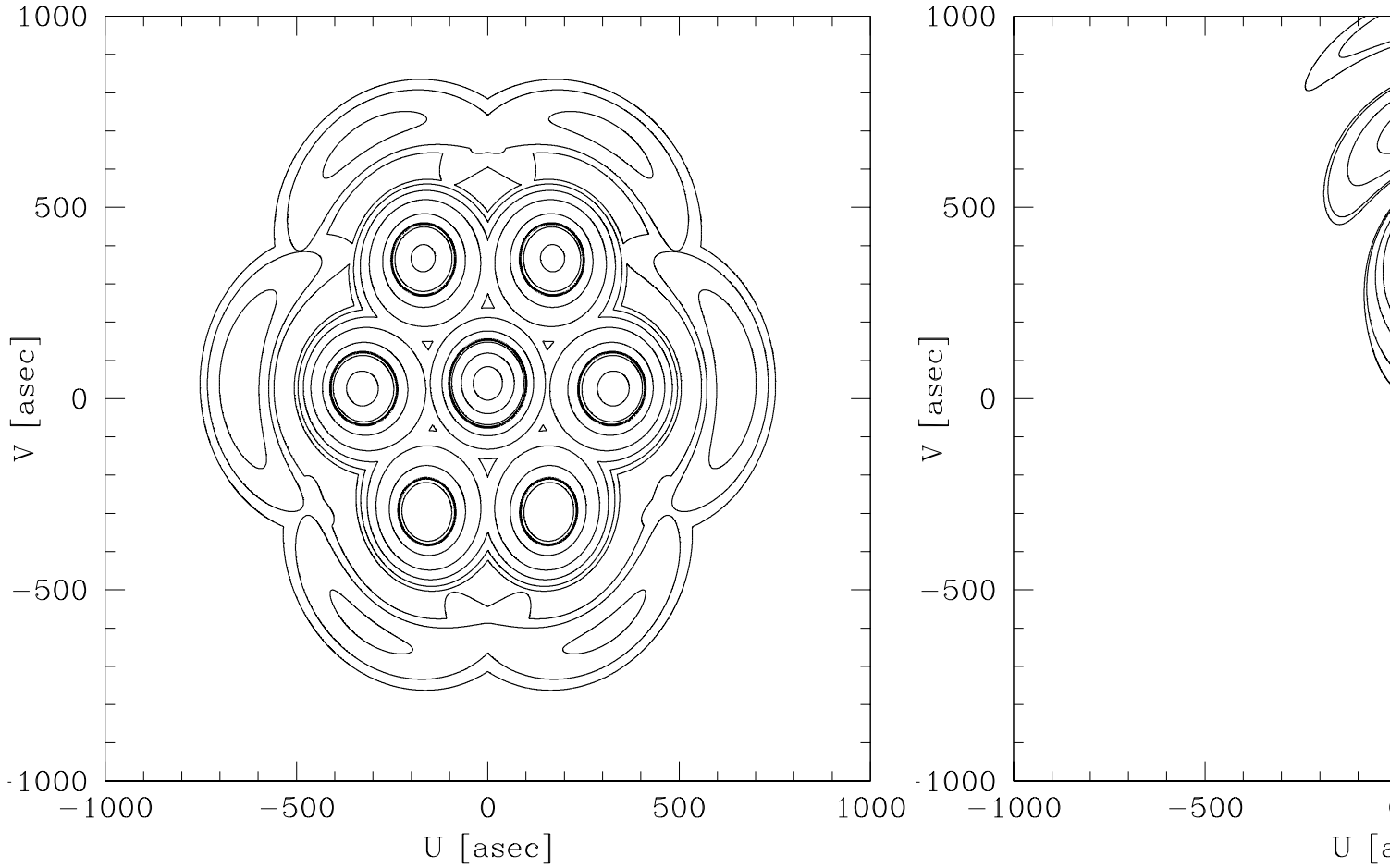


FIG. B5.— The footprint of the ALFA beams on the sky (left) and one of the single outer beams (right). For the complete beam pattern the contours are drawn at decibel levels of $-0.4, -1.4, -4.4, -7.4, -10.4$ and -13.4 and the thick contour denotes the half-power level. For the single beam additional contours are added at $dB = -16.4$ and -21.7 and the thick contour again denotes the half-power level.

of pulsars detected in the sidelobes is $\approx 6\%$. We can calculate the ratio between the volumes surveyed in the sparse and dense sampling schemes by evaluating:

$$V_{\max} \propto \int_{\Omega} d\Omega G^{3/2}(\Omega) \quad (\text{B1})$$

where G is the gain and Ω is the covered solid angle. We assume the same integration time for both schemes and integrate out to the half-power level for the dense sampling while integrating out past the first sidelobe for the sparse sampling. Then, as a result of the high sidelobes, the volume surveyed in the sparse sampling scheme is 1.73 times the volume surveyed with the same number of pointings of the dense approach.

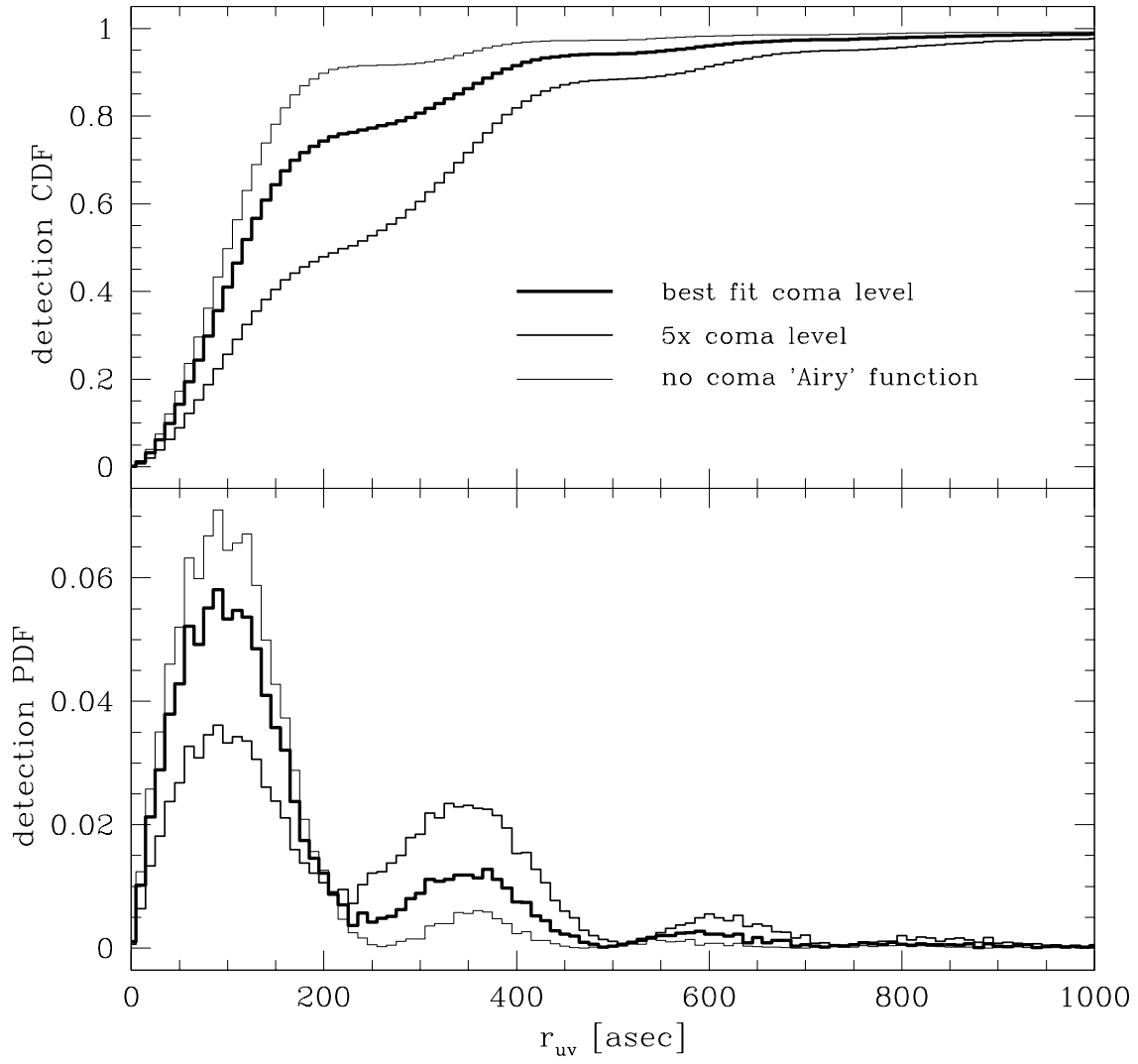


FIG. B6.— The detection PDF and CDF for the complete 7-beam ALFA system of the distance r_{uv} from the detected pulsar to the center of the beam in which that pulsar is detected. Pulsars detected in multiple beams are counted for each of those beams. The thick line corresponds to the actual ALFA beam, the intermediate line corresponds to a 5 times increase in coma level while the thin line corresponds to a beam system described by a regular Airy function.

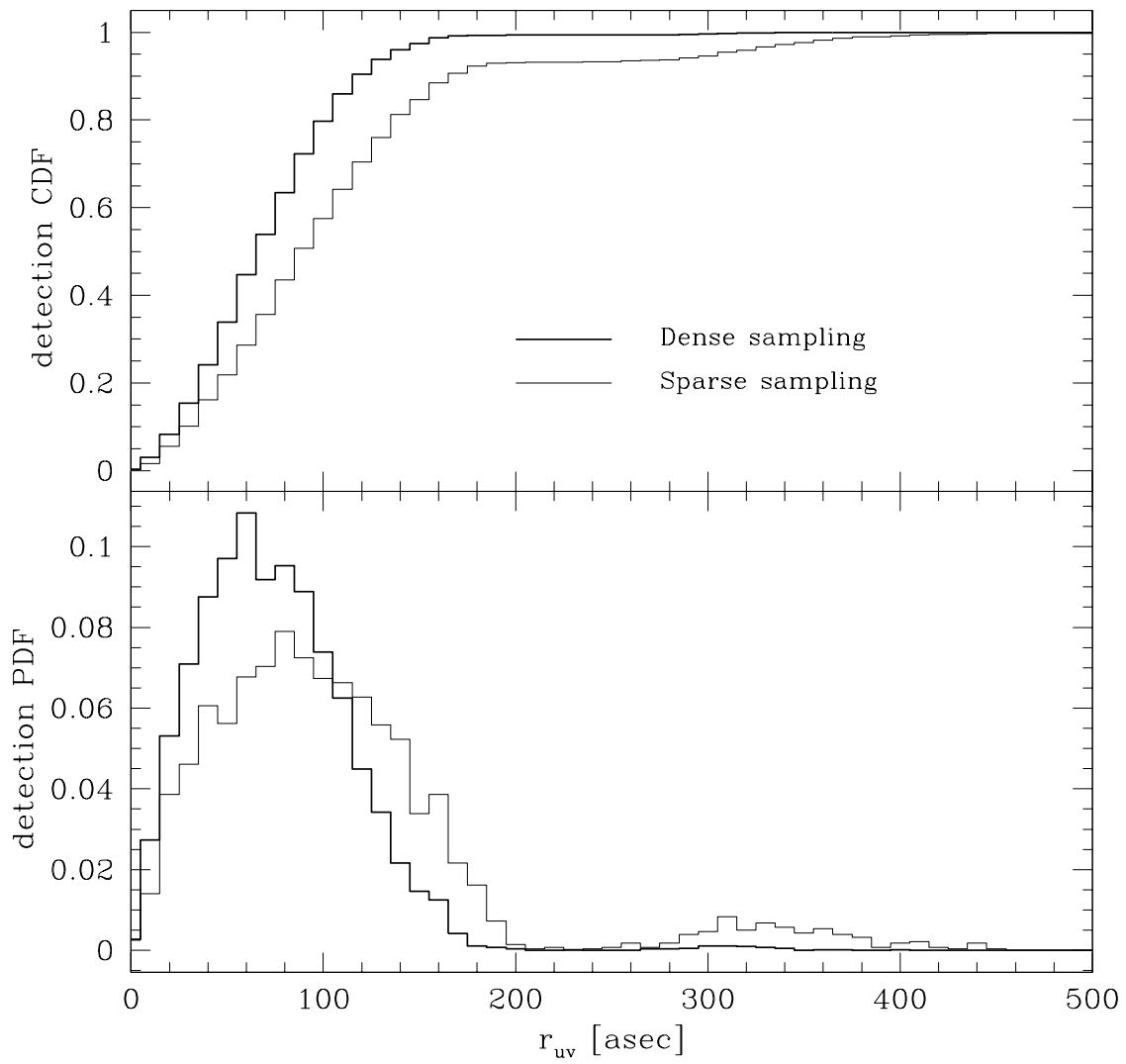


FIG. B7.— Similar to Fig. B7 for the actual ALFA beams, counting only the best of multiple detections (note the different scale). The thick line corresponds to the dense sampling scheme while the thin line corresponds to the sparse sampling scheme that makes use of detections in the sidelobes.